

# Polar Alignment of $\Lambda$ -Shaped Basic Building Units within Transition Metal Oxide Fluoride Materials

Michael Holland,<sup>†,‡</sup> Martin D. Donakowski,<sup>†,‡</sup> Eric A. Pozzi,<sup>†</sup> Andrew M. Rasmussen,<sup>†</sup> Thanh Thao Tran,<sup>§</sup> Shannon E. Pease-Dodson,<sup>†</sup> P. Shiv Halasyamani,<sup>§,||</sup> Tamar Seideman,<sup>†</sup> Richard P. Van Duyne,<sup>†</sup> and Kenneth R. Poeppelmeier<sup>†,\*</sup>

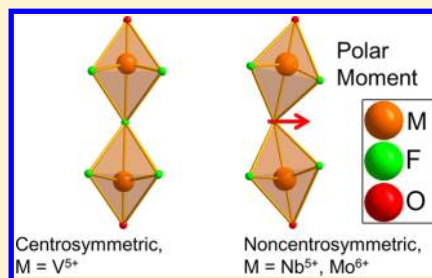
<sup>†</sup>Department of Chemistry, Northwestern University, 2145 Sheridan Road, Evanston, Illinois 60628-3113, United States

<sup>§</sup>Department of Chemistry, University of Houston, 136 Fleming Building, Houston, Texas 77204-5003, United States

<sup>||</sup>Department of Chemistry, Aalto University, Laboratory of Inorganic Chemistry, P.O. Box 16100, FI-00076 AALTO, Finland

## Supporting Information

**ABSTRACT:** A series of pseudosymmetrical structures of formula  $K_{10}(M_2O_nF_{11-n})_3X$  ( $M = V$  and  $Nb$ ,  $n = 2$ ,  $X = (F_2Cl)_{1/3}$ ,  $Br$ ,  $Br_{4/2}$ ,  $I_{4/2}$ ;  $M = Mo$ ,  $n = 4$ ,  $X = Cl$ ,  $Br_{4/2}$ ,  $I_{4/2}$ ) illustrates generation of polar structures with the use of  $\Lambda$ -shaped basic building units (BBUs). For a compound to belong to a polar space group, dipole moments of individual species must be partially aligned. Incorporation of  $d^0$  early transition metal polyhedral BBUs into structures is a common method to create polar structures, owing to the second-order Jahn–Teller distortion these polyhedra contain. Less attention has been spent examining how to align the polar moments of BBUs. To address alignment, we present a study on previously reported bimetallic BBUs and synthesized compounds  $K_{10}(M_2O_nF_{11-n})_3X$ . These materials differ in their (non)centrosymmetry despite chemical and structural similarities. The vanadium compounds are centrosymmetric (space groups  $P\bar{3}m1$  or  $C2/m$ ) while the niobium and molybdenum heterotypes are noncentrosymmetric ( $Pmn2_1$ ). The difference in symmetry occurs owing to the presence of linear, bimetallic BBUs or  $\Lambda$ -shaped bimetallic BBUs and related packing effects. These  $\Lambda$ -shaped BBUs form as a consequence of the coordination environment around the bridging anion of the metal oxide fluoride BBUs.



## INTRODUCTION

The synthesis of efficient second-harmonic generation (SHG) active crystals requires that the crystal belong to a noncentrosymmetric (NCS) crystal class.<sup>1–5</sup> Previous attempts to create NCS crystals have used chiral organic molecules, as the chirality is necessarily preserved within the bulk structure.<sup>6</sup> This method synthesizes organic molecular crystals that are symmetrically chiral and therefore SHG active. As described by Chen's anionic group theory, the most efficient SHG activity typically resides in crystals that belong to *polar* space groups, which are not necessarily chiral. Additionally, constructive arrangement of polar anions could increase nonlinear optical responses.<sup>7,8</sup> Early transition metals (ETMs) with  $d^0$  electron configurations are prone to undergo polar second-order Jahn–Teller (SOJT) distortions.<sup>9</sup> Such distortions and polar space groups are associated with the high SHG efficiencies of  $LiNbO_3$  and  $KTiOPO_4$ ; however, these isolated polar moments are not—in and of themselves—enough to create an SHG response within a material.

To belong to a polar space group, a crystal must have dipoles partially (or fully) aligned in such a way that a polar moment is expressed in the bulk. Typically, a polar anion will be oriented with a neighboring polar anion that has an equal but opposite dipole moment. This is energetically favorable as per Pauling's second rule, as this increases local electroneutrality.<sup>10</sup> This

often results in a centrosymmetric (CS) compound that cannot exhibit properties associated with NCS crystal classes such as SHG activity, pyroelectricity, piezoelectricity, and circular dichroism. Advances in solid-state chemistry have provided SHG-active crystals of high efficiency;<sup>11–17</sup> however, less attention has been spent looking at how a crystal can be stabilized within an NCS configuration.

Alignment can be approached by the examination of the coordination environment around an ETM basic building unit (BBU). For instance, octahedra of ETM oxide fluorides can have *cis*- and *trans*-directing properties owing to unequal electronic distributions arising from second-order Jahn–Teller effects.<sup>15,17</sup> These properties have allowed qualitative predictions of stable, crystallographic orientations for such octahedra. The use of  $\Lambda$ -shaped BBUs can increase the likelihood of forming a polar material.<sup>11,18</sup> This strategy has been previously used in organic crystallography, liquid crystals, and polymer science to synthesize SHG-active media.<sup>19–23</sup>

Creation of purely inorganic  $\Lambda$ -shaped units can be more difficult than organic chemical synthesis, as targeted syntheses of solid-state materials is less molecularly tailorable than organic chemistry. Previous research, particularly by Udovenko and

Received: August 27, 2013

Laptash, resulted in the synthesis of a variety of ETM oxide fluorides that contain  $[M_2O_nF_{11-n}]^{m-}$  BBUs, some of which are  $\Lambda$ -shaped.<sup>24–29</sup> These oxide fluorides are shown in Table 1. We also note that the fluoride–sulfide anion  $[W_2F_9S_2]^-$  has recently been reported.<sup>30</sup>

**Table 1. Previously Reported Structures in the Family  $A_{10}(M_2O_nF_{11-n})_3X$  and Others with  $[M_2O_nF_{11-n}]^{3-}$  Anions**

compound	space group	citation
$(NH_4)_3Nb_3O_3F_{14} \cdot H_2O^*$	$P6_3mc$	24
$K_3Nb_3O_3F_{14} \cdot H_2O^*$	$P6_3mc$	24
$Rb_3Nb_3O_3F_{14} \cdot H_2O^*$	$P6_3mc$	24
$Cs_3Nb_3O_3F_{14} \cdot H_2O^*$	$P6_3mc$	24
$(NH_4)_3(Mo_2O_2F_9)$	$P\bar{3}m1$	25
$Rb_{10}Nb_6O_7F_{26} \cdot H_2O$	$P3$	28
$K_{10}(Nb_2O_2F_9)_3F$	$Pmn2_1$	29
$(NH_4)_{10}(Nb_2O_2F_9)_3F$	$P\bar{3}m1$	29
$Rb_{10}(Nb_2O_2F_9)(F_2Cl)_{1/3}$	$P\bar{3}m1$	29
$Rb_{10}(Mo_2O_4F_7)_3F$	$P\bar{3}m1$	29
$Rb_{10}(W_2O_4F_7)_3F$	$P\bar{3}m1$	29

\*Space group was provided as most likely space group amongst three possibilities.

The compounds in Table 1 and the new compounds reported herein contain similar structures, but with markedly different space groups. Several of the structures in Table 1 have unit cells similar to those of the compounds we report here. This work presents one synthetic strategy toward the stabilization of  $\Lambda$ -shaped BBUs for the generation of NCS compounds. Namely, bimetallic BBUs in compounds of  $K_{10}(M_2O_nF_{11-n})_3X$  ( $M = V, Nb, n = 2$ ;  $M = Mo, n = 4$ ;  $X = (F_2Cl)_{1/3}, Cl, Br, ([Br_3][Br])_{1/2},$  and  $([I_3][I])_{1/2}$ ) show that when the bridging ion of these BBUs is underbonded, it will distort out of a center of symmetry. The underbonded nature derives from the specific electronic distribution around the ETM. Alteration of the ETM modifies the geometry and polarity of the bimetallic BBUs with little change of the extended network surrounding the BBUs. This comparison of structurally similar CS and NCS materials provides insight into the creation of NCS materials. These principles apply to the compounds of Table 1. We focus on structures with  $A^+ = K$  to examine the role of the *early transition metal* within CS and NCS crystal classes.

## EXPERIMENTAL METHODS

**Caution!** Hydrofluoric acid is toxic and corrosive! It must be handled with extreme caution and the appropriate protective gear and training.<sup>59–61</sup>

**Materials.** Hydrofluoric acid (49% HF by weight), potassium fluoride (>99.0%), and molybdenum oxide (99.5%) were used as received from Sigma-Aldrich. Niobium oxide (99.9985%, trace metals basis), vanadium oxide (99.6%), and potassium bromide (99+%) were obtained from Alfa-Aesar. Potassium chloride (99.48%) was obtained from Mallinckrodt. Deionized water was used in reagent quantities and as backfill in the pressure vessels. Teflon pouches of poly(tetrafluoroethylene) were made as previously described.<sup>13,31,32</sup>

**Synthesis and Isolation of Single Crystals.** The crystals of  $K_{10}(M_2O_nF_{11-n})_3X$  were synthesized by hydrothermal methods: 10 mmol  $KX$  ( $X^- = F, Cl, Br, I$ ), 1 mmol  $M_2^{5+}O_5$  ( $M^{5+} = V, Nb$ ) or 2 mmol  $M^{6+}O_3$  ( $M = Mo^{6+}$ ), 24 mmol HF (0.87 mL of 49% HF in water by weight), and 0.63 mL of

deionized water were placed within a Teflon pouch and sealed with an impulse sealer. Compounds with tribromide species were synthesized by adding an additional 5 mmol of KBr. The starting reagents did not contain  $[X_3]^-$ ; therefore, the hydrothermal syntheses generated  $[X_3]^-$  through oxidative processes at elevated temperature and pressure. We speculate that oxidative species are present in the  $HF_{aq}$  that may facilitate the oxidation of  $3[X]^- \rightarrow [X_3]^-$ .  $K_{10}(V_2O_2F_9)_3(F_2Cl)_{1/3}$  was initially synthesized with solely  $V_2O_5$ , KF,  $HF_{aq}$ , and deionized water (e.g., no chloride source). We examined the starting materials  $V_2O_5$  and KF with energy dispersive X-ray spectroscopy (EDS) but found no chloride impurities. The chloride impurities may derive from the deionized water or  $HF_{aq}$  used. Subsequently, the compound was made with 10/3 mmol of KCl and 20/3 mmol of KF. These pouches were then placed, alone, within Teflon-lined Parr acid digestion vessels and heated to 150 °C, held at this temperature for 24 h, and then cooled to 25 °C at 0.1 °C/min. The pouches were then opened and the crystals were then filtered in air. The products that contain trihalide ions are a 50:50 mixture of monohalide and trihalide ions ( $[X]_{1/2}^-$  and  $[X_3]_{1/2}^-$ ), and we subsequently denote their content as  $([X_3][X])_{1/2}$ .

**Elemental Analysis.** To evaluate the amount of halide ions within the structures, we performed energy dispersive X-ray spectroscopy (EDS). The data were obtained on a Hitachi S340N-II SEM with an accelerating voltage of 20 keV and analyzed over the range 0–10 keV with the use of INCA software. The elemental analysis corresponds to the atomic content of the materials (see Supporting Information).

**Crystallographic Determination.** We obtained single crystal XRD data at 100 K with the use of a Bruker Kappa Apex 2 CCD diffractometer with monochromated  $Mo\ K\alpha$  radiation ( $\lambda = 0.71073 \text{ \AA}$ ). The crystal-to-detector distance was 60 mm. The data were then integrated with the program SAINT-V7.23A.<sup>34</sup> Face-indexed absorption corrections were applied to untwinned crystal data. The structures were determined with XS by identification of the metallic ions with direct methods of Fourier syntheses and then refined with ShelXL to determine the anion sites within the Olex2 suite.<sup>35,36</sup> The structure was checked with PLATON, and no additional symmetry elements were found.<sup>37</sup> Crystals that contained twin domains were corrected for absorption with TWINABS.<sup>35</sup> Powder XRD data and associated impurity discussions are located in the Supporting Information.

**Computational Geometry Optimizations.** Geometry optimizations were performed for (i) the  $\Lambda$ -shaped geometry of the  $[Nb_2O_2F_9]^{3-}$  BBU, (ii) a linear geometry of the  $[Nb_2O_2F_9]^{3-}$  BBU with the crystallographic coordinates of the linear  $[V_2O_2F_9]^{3-}$  BBU, and (iii) the same linear coordinates with the central atom displaced by 0.1 Å perpendicular to the central axis. The optimizations were performed with the Q-Chem 4.1 computational chemistry package comparing three pseudopotentials (CRENBL, LANL2DZ, SBKJJC) and four different exchange-correlation functionals (PBE0, TPSSH, M06, M11).<sup>38</sup> The output optimized geometries of the  $[Nb_2O_2F_9]^{3-}$  BBU are independent of the basis and functional used to within less than a degree in the Nb–F–Nb angle, 0.05 Å in the Nb-bridge F and Nb-axial F distances, and 0.1 Å in the Nb–O distance (see Table S2 in the Supporting Information).

**Second-Harmonic Generation.** To verify compounds 3–8 crystallize in an NCS space group ( $Pmn2_1$ ), we measured the SHG response of compound 3 as a representative example (Figure 1). Powder SHG measurements using 1064 nm

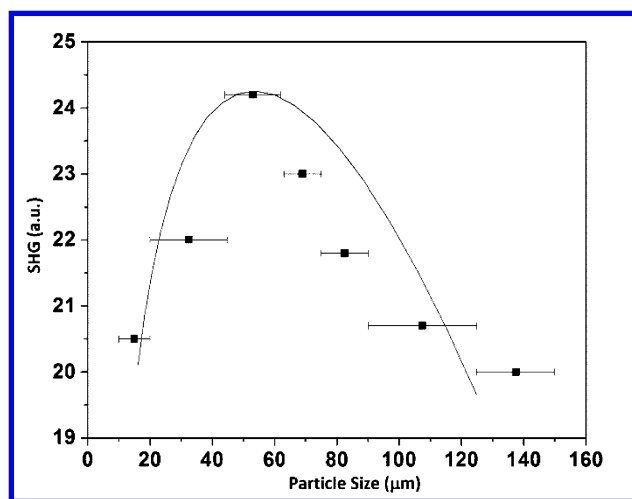


**Figure 1.** Second-harmonic generation response (arbitrary units) plotted versus particle size of a representative sample ( $K_{10}(\text{Mo}_2\text{O}_4\text{F}_7)_3\text{Cl}$ ). The compound exhibits a response approximately 30 times that of  $\alpha\text{-SiO}_2$  and is type 1 nonphase-matchable. The line drawn is to guide the eye and is not a fit of the data.

radiation revealed an SHG efficiency of approximately  $30 \times \alpha\text{-SiO}_2$  in the 45–63  $\mu\text{m}$  particle size range. Additional SHG measurements of the particle size vs SHG efficiency showed compound 3 exhibits type 1 non-phase-matchability. As such,  $K_{10}(\text{Mo}_2\text{O}_4\text{F}_7)_3\text{Cl}$  falls into the class C category of SHG materials, as defined by Kurtz and Perry.<sup>33</sup> Based on these measurements, we estimate an average NLO susceptibility,  $\langle d_{\text{eff}} \rangle_{\text{exp}}$  of approximately 3.0 pm/V.

**Resonance Raman Spectroscopy.** Resonance Raman spectroscopy was performed using a Nikon Eclipse Ti2000-U inverted microscope into which a 532 nm continuous-wave laser (Spectra-Physics Millennia Pro) was coupled. A 20 $\times$  extra-long working distance objective (NA = 0.45) focused the 6.5 mW incident beam onto the stationary samples, which were situated in air atop #1.5 glass coverslips. The same objective collected scattered light, which was then focused onto the 250  $\mu\text{m}$  entrance slit of a TriplePro three-stage spectrograph and detected by a liquid  $\text{N}_2$ -cooled Spec-10:400BR charge-coupled device (Princeton Instruments) such that low energy modes could be observed. Spectra of compounds 2, 7, and 8 were acquired for 20 s and accumulated 3 times, and spectra of

compounds 5 and 6 were acquired for 5 s and accumulated 12 times.

## BOND VALENCE CALCULATIONS

Selected bond valence values are shown in Table 2 while more complete tables of bond valence calculations are available in the Supporting Information. Individual bond valence values were calculated using eq 1,<sup>39–42</sup>

$$S_{ij} = \exp[(R_0 - R_{ij})/B] \quad (1)$$

where  $S_{ij}$  is the valence of the bond  $ij$ ,  $R_{ij}$  is the length of the bond  $ij$ , and  $R_0$  and  $B$  are empirical constants dependent on the identity of the  $i$  and  $j$  bonded elements. Bond valence values arrived at by this method are not applicable for bonds to disordered sites or sites of partial occupancy, and such bonds are not included in our calculations.

## RESULTS

The compounds we synthesized of formulas  $K_{10}(\text{M}_2\text{O}_n\text{F}_{11-n})\text{X}$  contain similar structures but crystallize in three different space groups:  $P\bar{3}m1$ ,  $C2/m$ , and  $Pmn2_1$ . Each structure has two symmetrically distinct bimetallic BBUs around channels that contain disordered halide ions that have elongated ellipsoids and/or are distributed over multiple sites. Figures 2–4 show

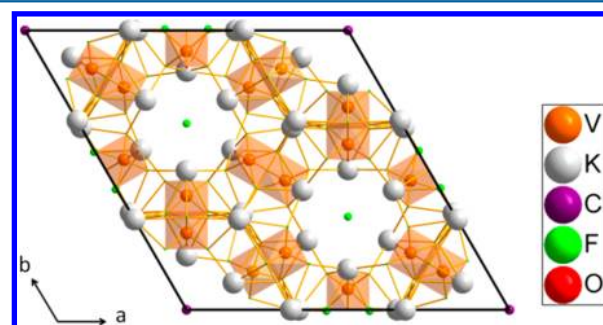


**Figure 2.** View of the  $P\bar{3}m1$  structure of  $K_{10}(\text{V}_2\text{O}_2\text{F}_9)_3(\text{F}_2\text{Cl})_{1/3}$  along the  $c$  axis. The halogens ( $X = \text{Cl}^-$  and  $\text{F}^-$ ) are within the pores and weakly coordinate to the surrounding potassium cations.

the compounds down the axis along which the disordered halide channels lie. The compounds contain halide ions that are distributed along these channels: a Fourier difference map demonstrating this is provided in the Supporting Information.

**Table 2.** Selected Bond Lengths, Bond Valence Calculations, and Environment of the Bridging Fluoride Ligands for BBUs of Representative Compounds from Each Space Group

compoundspace group	$i\text{-}j^a$	$R_{ij}^b$	$S_{ij}^c$	$\text{NC}^d$	$\text{PC}^e$	bridging angle (deg)
$K_{10}(\text{Nb}_2\text{O}_2\text{F}_9)_3\text{I}_2$ $Pmn2_1$	Nb1-F9	2.178(6)	0.389	0.244	0.162	164.1(3)
	Nb2-F9	2.200(2)	0.367			
	Nb3-F14	2.227(6)	0.341	0.284	0.193	160.3(3)
	Nb4-F14	2.192(6)	0.375			
$K_{10}(\text{V}_2\text{O}_2\text{F}_9)_3([\text{Br}_3][\text{Br}])_{1/2}$ $C2/m$	V1-F4	2.1307(8)	0.341	0.318	0.272	180
	V2-F8	2.1084(11)	0.360	0.280	0.295	180
$K_{30}(\text{V}_2\text{O}_2\text{F}_9)_9\text{F}_2\text{Cl}$ $P\bar{3}m1$	V1-F3	2.134(6)	0.384	0.278	0.255	168.4(3)
	V2-F3	2.083(6)	0.338			
	V3-F6	2.0756(14)	0.391	0.218	0.265	180

<sup>a</sup>Bonding species in the structure. <sup>b</sup>Observed bond length ( $\text{\AA}$ ). <sup>c</sup>Calculated bond valence. <sup>d</sup>Residual negative charge left on the bridging fluoride anion after accounting for the bond valence contribution by the transition metal bonds. <sup>e</sup>Positive charge contributed to the anion by coordinating  $\text{K}^+$  ions.

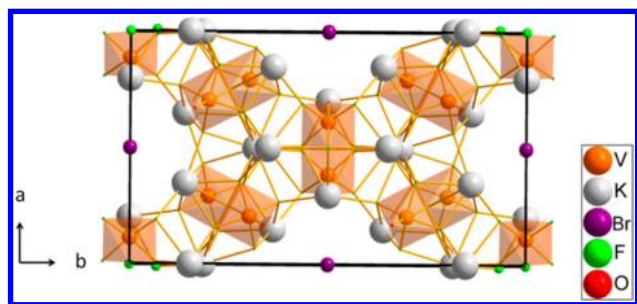


**Figure 3.**  $C2/m$  structure of  $K_{10}(V_2O_2F_9)[Br_3 Br]_{1/2}$  viewed along the  $c$  axis. In this work, the halogens are disordered along the polar axis and consist of  $X = Br^-$  and  $Cl^-$ .

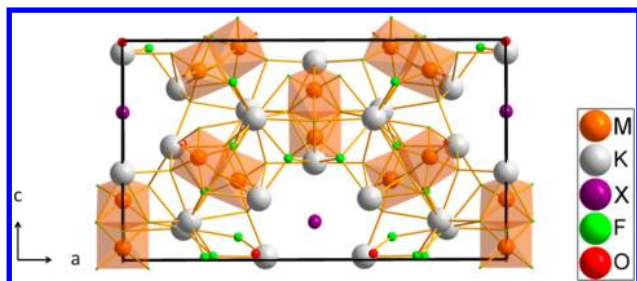


**Figure 4.**  $Pmn2_1$  structure of  $K_{10}(M_2O_nF_{11-n})X_3$  ( $M = Nb^{5+}$ ,  $Mo^{6+}$ ) viewed along the  $b$  axis. This structure is present for two early transition metals:  $M = Nb^{5+}$ ,  $a = 2$ ,  $b = 9$ ;  $Mo^{6+}$ ,  $n = 4$ . For clarity, oxide-fluoride disorder of the molybdate species are not illustrated.

Such disordered channels could be of interest for solid-state electrolytes for halide ions.<sup>43</sup> The halides coordinate solely to potassium cations that make up the framework of the channels. These potassium cations lie between the halide ions and the bimetallic BBUs. These BBUs exist as  $[M_2O_nF_{11-n}]^{3-}$  anions ( $M = V^{5+}$ ,  $Nb^{5+}$   $n = 2$ ;  $M = Mo^{6+}$   $n = 4$ ). As has been previously observed, oxide fluoride molybdate compounds have two oxide ions per metal center: one coordinated terminally and one disordered among the four equatorial positions.<sup>44</sup> This is the case, based upon charge balance, for  $K_{10}(Mo_2O_4F_7)_3X$  ( $X = Cl$ ,  $([Br_3][Br])_{1/2}$ ,  $([I_3][I])_{1/2}$ ). Compound 3 has an octahedron torsionally angled by  $45^\circ$  relative to its bridged octahedron. The equatorial fluoride ions are thus staggered along the M–F–M axis of this one BBU.

Computational geometry optimizations predict a tendency for the oxide fluoride building unit to adopt a linear configuration independent of the influence of the surrounding crystal environment. In particular, it is clear that the Nb–F–Nb component is linear independently of the basis set used. Averaged over all optimized geometries, the average (standard deviation) Nb-bridging F–Nb angle is  $179.36^\circ$  ( $1.60^\circ$ ), the Nb-bridging F bond distance is  $2.24 \text{ \AA}$  ( $0.01 \text{ \AA}$ ), the Nb-axial F bond distance is  $1.99 \text{ \AA}$  ( $0.01 \text{ \AA}$ ), and the Nb–O bond distance is  $1.77 \text{ \AA}$  ( $0.01 \text{ \AA}$ ).

Unit cell determination was ambiguous, as crystallographic data could each fit the three unit cells; subsequent refinement was used to determine the correct unit cell. As shown in Figure 5, the three structures are “pseudosymmetrical” in that they have very similar placement of atoms, but subtle changes that exist of the atomic coordinates place the structures in different, sometimes polar, space groups. The compound  $K_{10}(Mo_2O_4F_7)_3Br_{2/2}$  showed commensurate modulation with use of the  $Cmc2_1$  cell setting and modulation vector  $q = (0, 1/3, 0)$ . The commensurate structure occurs on account of two

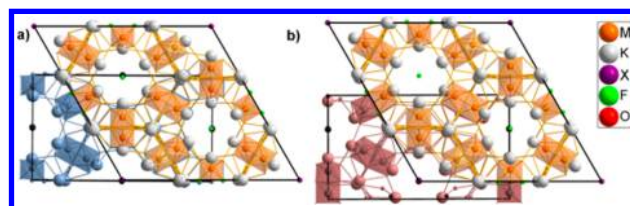


**Figure 5.** Comparison of the three structure types observed in the pseudosymmetrical structures:  $K_0(V_2O_2F_9)_3(F_2Cl)_{1/3}$  crystallizes in a trigonal configuration (space group  $P\bar{3}m1$ ). The early transition metal and halogen ions can alter the crystal lattice subtly so that the crystal has (a) monoclinic symmetry  $C2/m$  or (b) orthorhombic symmetry,  $Pmn2_1$ .

channels in a 1:1 ratio of  $[Br^-]/[Br_3^-]$ . This structure is provided in the Supporting Information, but the modeled structure in space group  $Pmn2_1$  is presented for comparative reasons.

Figure 4 shows compounds 4–8 within the NCS space group  $Pmn2_1$ . The similarities between the three structure-types are shown in Figure 5. Table 3 summarizes the chemical formulas and crystallographic cell parameters for the 8 new compounds we synthesized for this paper. Compounds 1 and 2 consist of  $M = V^{5+}$  and have CS crystal structures. Figure 2 shows that compound 1 has the highest symmetry (trigonal, space group  $P\bar{3}m1$ ). This compound is notable in that it contains two pores of different sizes: one that has an ordered chloride ion and one that has a disordered fluoride anion. Compound 2 belongs to the monoclinic space group  $C2/m$  with one size of pores to accommodate the bromide anions (Figure 3).

As mentioned, significant disorder exists within the one-dimensional halide channels. To examine this, we performed pair-distribution function (PDF) measurements in an attempt to resolve or confirm disorder. Significant disorder does exist in the compounds (evidenced by broad peaks of high intensity), and adequate fits were performed using X-ray crystallographic parameters with the obtained PDF data (see Supporting Information).

The presence of triiodide ions in compounds 7 and 8 and tribromide ions in compounds 2, 5, and 6 was confirmed with resonance Raman spectroscopy (Figure 6). Observed fundamental (symmetric stretch,  $\nu_1$ ) band frequencies agree with previous reports of trihalide detection.<sup>45–49</sup> Additionally, the characteristic overtone progressions of triiodide ions and tribromide ions can be visualized in each spectrum at roughly integer multiples of their respective  $\nu_1$  frequencies, consistent with previous Raman studies performed on resonance.<sup>50</sup> Interestingly, a prominent feature to the red of the  $[Br_3^-]$  fundamental is present in the spectra of each of the bromine-containing compounds. We attribute this peak to the  $[Br_3^-]$  asymmetric stretch,  $\nu_2$ , which becomes Raman active as a result of distortion due to crystal forces.<sup>51,52</sup>

## DISCUSSION

The structure of ETM oxide/oxide fluoride BBUs are governed by primary and secondary distortions.<sup>42</sup> The primary distortion refers to SOJT effects, and the secondary distortion arises from the nature of the coordination between the BBU and the extended network. The similarity of the structures (particularly compounds  $K_{10}(M_2O_nF_{11-n})_3([Br_3][Br])_{1/2}$ : Compounds 2, 5, and 6) allows identification of the influences that stabilize  $\Lambda$  BBUs in some cases and linear BBUs in others. The  $[M_2O_nF_{11-n}]^{3-}$  BBUs are composed of two corner-sharing

Table 3. Space Group and Cell Parameters for Compounds  $K_{10}(M_2O_nF_{11-n})_3X$ 

compound	1	2	3	4	5	6	7	8
space group	$P\bar{3}m1$	$C2/m$	$Pmn2_1$	$Pmn2_1$	$Pmn2_1$	$Pmn2_1$	$Pmn2_1$	$Pmn2_1$
<i>a</i>	19.2623(6)	11.2978(3)	19.907(2)	20.1125(11)	20.0779(6)	20.0790(6)	20.3471(6)	20.0720 (8)
<i>b</i>	19.2623(6)	19.1761(5)	7.7643(10)	7.7382(4)	7.7588(2)	7.7580(2)	7.8376(3)	7.7549(3)
<i>c</i>	7.7318(2)	7.7624(2)	11.2139(14)	11.4797(6)	11.48289(4)	11.4836(3)	11.6367(3)	11.4644(4)
$\beta$ (deg)	120	93.247(1)	90	90	90	90	90	90
r1	0.0613	0.0332	0.0425	0.0290	0.0305	0.0434	0.0434	0.0427
wR2	0.1774	0.0977	0.1130	0.0844	0.0850	0.1421	0.1088	0.1186
GoF	1.132	1.157	1.033	1.170	1.174	1.231	0.949	1.067

<sup>a</sup>Exhibits commensurate supersymmetry; structure is presented in the Supporting Information.

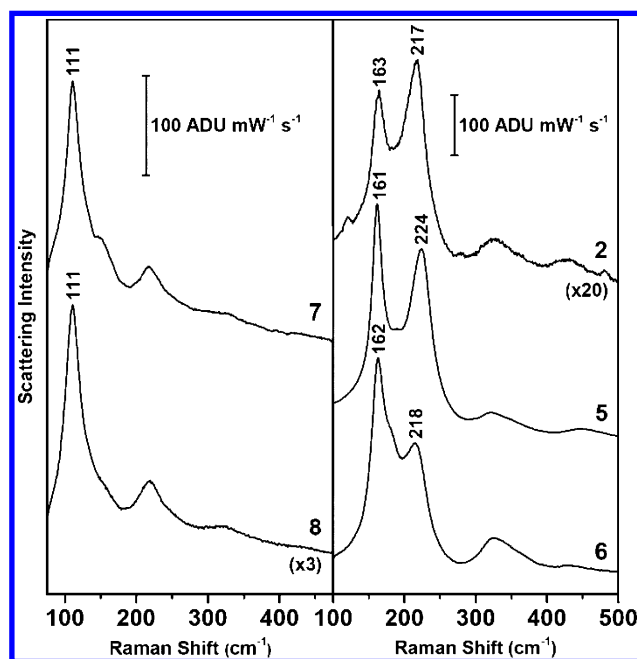
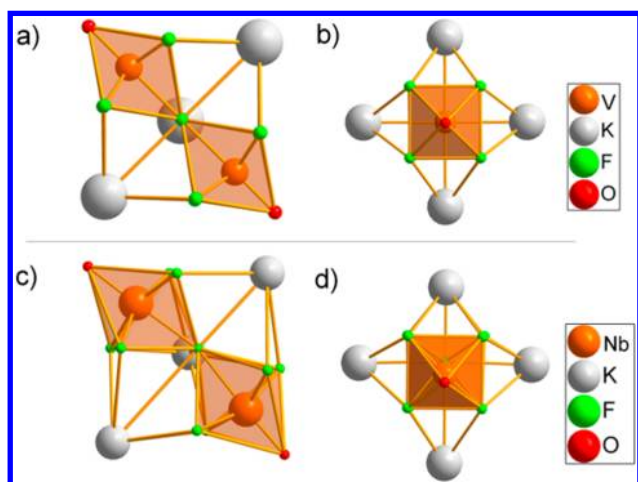


Figure 6. Resonance Raman spectra confirming the presence of  $[I_3]^-$  in compounds 7 and 8 and  $[Br_3]^-$  in compounds 2, 5, and 6. Spectra were acquired with  $\lambda_{ex} = 532$  nm,  $P_{ex} = 6.5$  mW, and  $t_{aq} = 30$  s [3 accumulations (compounds 2, 7, and 8)] or with  $t_{aq} = 5$  s [12 accumulations (compounds 5 and 6)].

octahedra and a bridging fluoride ion trans to oxide anions in both octahedra. The primary distortions cause the ETMs to shift significantly away from the bridging fluoride anion.

The  $M=O$  bond for  $M = V^{5+}$  is considerably shorter and fulfills a large portion of the valence for both the oxide and vanadium ions (most  $V=O$  bonds  $>1.8$  valence units). This results in relatively longer  $M-F$  bonds (both equatorial and bridging fluoride ions). The  $M=O$  valences for  $M = Nb^{5+}$ ,  $Mo^{6+}$  are less (most  $Nb=O$  and  $Mo=O$  bonds  $<1.8$  valence units), and subsequently, the  $Nb^{5+}$  and  $Mo^{6+}$  shorten their  $M-F$  bonds to maintain a greater valence.<sup>53–55</sup> These  $M=O$  and  $M-F$  interactions are therefore correlated; however, we find that the bridging fluoride of the  $[V_2O_2F_9]^{3-}$  anion is more fulfilled as compared to the  $[M_2O_nF_{11-n}]^{3-}$  ( $M = Nb^{5+}$ ,  $n = 2$ ;  $Mo^{6+}$ ,  $n = 4$ ). This occurs on account of the electron distribution that arises from SOJT effects of the specific ETMs, as has been described by Welk et al. and Izumi et al.<sup>53,54</sup> The valences of the bridging fluoride anions in vanadium building units are more fulfilled when compared to those in niobium and molybdenum units.<sup>44,53,54,56</sup> The vanadium octahedra have shorter equatorial bonds as compared to the molybdenum and niobium octahedra. Subsequently, within compounds 1 and 2, the equatorial fluoride ions are tightly bonded to the vanadium, and in compounds 3–8, the equatorial fluorides are less closely bonded to the niobium and molybdenum metal centers. Figure 7 and Table 4 show that, for the vanadium species, the shorter  $V-F_{eq}$  bonds allow the surrounding potassium cations to more completely fulfill the valence of the bridging fluoride anion. For the niobium and molybdenum species, however, this is more difficult, owing to the greater  $M-F_{eq}$  bond length.

Two sets of these symmetry distinct  $[M_2O_nF_{11-n}]^{3-}$  BBUs are present in all structures. The specific coordination environment of the bridging fluoride anion dictates the  $M-F-M$  bond angle. The  $\Lambda$  shape allows the bridging fluoride anion to coordinate more closely to one potassium cation



**Figure 7.** (a) A linear, bimetallic vanadium BBU ( $M = V^{5+}$ ). The bond angle of  $V-F-V$  is symmetrically constrained to  $180^\circ$ . (b) Bimetallic vanadium BBU of compound **2** viewed down the  $V-F-V$  axis. Potassium cations have similar distances from the central fluoride ion. (c) View of the  $\Lambda$ -shaped bimetallic BBU ( $M = Nb^{5+}, Mo^{6+}$ ). The fluoride anion distorts from the center of the four coordinating potassium cations to satisfy its valence; consequently, the BBU forms a  $\Lambda$  shape. (d) View of bent BBU ( $M = Nb^{5+}, Mo^{6+}$ ) viewed down the  $M-F-M$  axis. The fluoride anion distorts from the center of the four potassium cations to satisfy its valence, forming a  $\Lambda$  shape.

without the cation overbonding to equatorial fluoride anions; consequently, this makes the bridging fluoride ion less severely underbonded.

The distortion theorem explains the stabilization of the  $\Lambda$  shapes in terms of bond valences. The variation of bond distances between the bridging fluoride anions and potassium cations provides stability. The distortion theorem, as applied to the bond valence method, states that, for a group of bonds of the same type, larger standard deviations of bond length require larger average distances to maintain the same valence sum.<sup>57</sup>

For a consistent average bond length, the bond valence sum increases as the uniformity of the bond lengths decreases. Each bridging fluoride anion coordinates to four potassium cations—all of which sit in the same plane. The short bonds between the vanadium and equatorial fluoride ions allow the surrounding

potassium ions to approach the bridging fluoride ion more closely. This provides sufficient valence for the bridging fluoride. The longer equatorial bonds for molybdate and niobate BBUs prevent such a close approach. The increased average distance from these cations to the bridging fluoride anion results in a decreased net valence contribution to the fluoride anion. The valence requirement of the bridging fluoride ion is better satisfied in these cases by distorting away from the center of the potassium cations.

The BBU becomes more stable with an increase in the net valence contribution between the potassium cations and the bridging fluoride anion. An isotropic, stabilizing environment around the bridging fluoride anion in the vanadate compounds creates CS BBUs that result in a CS structure. In contrast, it is the presence of an underbonded, destabilizing environment about the bridging fluorides that makes the out-of-center distortion preferred in these compounds and results in the NCS structures of the niobate and molybdate compounds.

Both sets of symmetry distinct  $[M_2O_nF_{11-n}]^{3-}$  BBUs in the NCS compounds have their net polar moment partially oriented along the  $c$  axis. The CS compound **2** contains two linear BBUs while the CS compound **1** contains one linear BBU and one  $\Lambda$ -shaped BBU. The linear BBUs of compound **2** are centrosymmetric and generate centers of symmetry. The bridging fluoride ion in the linear BBUs is less underbonded than that in the other transition metal BBUs. There is a small variation in the metal-to-fluoride ion distances between the different ETMs. Within the  $[V_2O_2F_9]^{3-}$  BBUs, fluoride anion bonds to the vanadium cation are  $\sim 0.1$  Å shorter than those of other BBUs (see Table 2). This abbreviated metal–equatorial fluoride ion bond distance allows the potassium cations to coordinate more closely to the bridging fluoride anion in the vanadate BBUs than in the molybdate or niobate BBUs. The bridging fluoride anion is therefore less underbonded in the vanadate compounds.

The  $\Lambda$ -shaped BBUs of compound **1** result from a different effect than the  $\Lambda$  shape in the niobium and molybdenum compounds: the presence of two different halide channels ( $[Cl]^-$  and  $[F]^-$ ). The larger ionic radii of  $[Cl]^-$  compared to  $[F]^-$  causes the potassium to pack more closely to the bridging fluoride, increasing the interaction toward the potassium and

**Table 4.** Bending of BBUs in Compounds, Showing the Angle of the  $\lambda$  Bend, the Bond Valence Contributions (in Valence Units) from the Transition Metal Centers, and the Bond Valence Sum Contribution from the Coordinating Potassium Cations

compound	bridging fluoride	M–F–M angle ( $^\circ$ )	BVS from ETMs	BVS from $K^+$ ions	BVS total
$K_{30}(V_2O_2F_9)_9F_2Cl$ ( <b>1</b> )	F3	168.443(314)	0.722	0.255	0.977
$K_{10}(V_2O_2F_9)_3([Br_3][Br])_{1/2}$ ( <b>2</b> )	F6	180	0.782	0.265	1.047
	F5	180	0.682	0.272	0.954
$K_{10}(Mo_2O_4F_7)_3Cl$ ( <b>3</b> )	F8	180	0.718	0.297	1.015
	F9	168.259(209)	0.765	0.201	0.966
$K_{10}(Nb_2O_2F_9)_3Br$ ( <b>4</b> )	F14	154.038(262)	0.740	0.206	0.946
	F9	160.841(168)	0.749	0.190	0.939
$K_{10}(Nb_2O_2F_9)_3([Br_3][Br])_{1/2}$ ( <b>5</b> )	F14	157.934(236)	0.708	0.243	0.951
	F9	161.010(252)	0.741	0.199	0.940
$K_{10}(Mo_2O_4F_7)_3([Br_3][Br])_{1/2}$ ( <b>6</b> )	F14	157.469(340)	0.708	0.247	0.955
	F2	160.633(291)	0.696	0.202	0.898
$K_{10}(Nb_2O_2F_9)_3([I_3][I])_{1/2}$ ( <b>7</b> )	F14	157.994(350)	0.673	0.246	0.918
	F9	164.057(262)	0.755	0.162	0.917
$K_{10}(Mo_2O_4F_7)_3([I_3][I])_{1/2}$ ( <b>8</b> )	F14	160.296(302)	0.716	0.193	0.909
	F2	168.271(209)	0.759	0.218	0.977
	F14	165.027(333)	0.714	0.251	0.964

chloride ions. As this packing effect is caused by an ion that is central to the BBUs, an inversion center is generated on the chloride ion and a CS material results.

Despite the parity of the selection of compounds we present, where vanadate compounds are CS while niobate and molybdate compounds are NCS, we note that the previously reported compounds of Table 3 [ $A_{10}(M_2O_nF_{11-n})_3X$  ( $A = (NH_4)^+, Rb^+, Cs^+$ ;  $M = Nb^{5+}, Mo^{6+}, W^{6+}$ ;  $X = F, (F_2Cl)_{1/3}$ )] contain nonvanadium ETMs that crystallize in the CS heterotype structure of  $P\bar{3}m1$ . Therefore, the CS or NCS structure formation is greatly influenced by the identity of the ETM, but the ammonium or alkali cations and other factors can also impact crystal packing and overall symmetry. As evidenced by compound 1, the presence of  $\Lambda$ -shaped moieties does not guarantee an NCS crystal structure but rather increases the probability of generating an NCS structure as it decreases the possible number/sites of inversion centers. Further computational experiments would facilitate an understanding of why the  $\Lambda$ -shaped BBUs in compounds 3–8 partially orient in one direction.

The calculated bond valence sums (bonds between ordered atomic sites of full occupancy) quantitatively explain stabilization of the  $\Lambda$ -shaped molybdenum and niobium BBUs. Table 4 shows the angle of the M–F–M bond of the BBUs in each compound and the bond valence contributions on the bridging fluoride anion. Within the compounds, a smaller angle (more pronounced  $\Lambda$ -shape) corresponds with a smaller bond valence contribution from the metal centers and a resulting lower BVS on the bridging fluoride. This is not observed, however, in the BBUs of compound 2—the environments of vanadium oxide fluorides can exhibit greater variance as compared to other  $d^0$  ETMs.<sup>53</sup>

In previous descriptions of early transition metal oxide fluorides, the SOJT distortion can primarily distort toward a corner ( $V^{5+}, Nb^{5+}$ ) or an edge or face ( $Mo^{6+}$ ). Computational geometry optimizations were performed to examine if the  $\Lambda$  shape of the bimetallic BBUs was caused by primary SOJT distortions or if the distortion was holistically caused by the overall structure of the material (e.g., a distortion induced by the positioning of potassium cations with respect to the BBUs). Previous computational examinations of the ion  $[Tc_2O_2F_9]^+$  showed the ion inherently has a  $\Lambda$ -shape.<sup>58</sup> Geometry optimizations were performed on linear (using coordinates for  $[V_2O_2F_9]^{3-}$  with  $Nb^{5+}$  substituted for  $V^{5+}$ ) and  $\Lambda$ -shaped  $[Nb_2O_2F_9]^{3-}$  BBUs. Regardless of whether the BBUs begin as linear or  $\Lambda$ -shaped, the geometry-optimized anion is linear without the presence of the overall structure. Therefore, the polar nature of the BBUs is induced by the overall crystal structure and not the bimetallic units alone. Detailed examinations of complex packing phenomena throughout compounds are required to elucidate the principles of creating NCS compounds for NLO applications; with these learned principles, targeted syntheses can be attempted.

## CONCLUSION

A series of compounds  $K_{10}(M_2O_nF_{11-n})_3X$  ( $M = V^{5+}, Nb^{5+}$ ;  $n = 2$ ;  $M = Mo^{6+}$ ;  $n = 4$ ;  $X = F_2Cl, Cl, Br, ([Br_3][Br])_{1/2}, ([I_3][I])_{1/2}$ ) illustrates the nucleophilicity of early transition metals and its resulting effect on the geometry and symmetry of a structure. The compounds consist of an oxide-fluoride framework of transition metal cations, potassium cations, and halides; the potassium cations create porous channels that contain highly disordered halide anions. A significant parity was

found in these compounds: when  $M = Nb^{5+}$  or  $Mo^{6+}$ , the compound is polar (space group  $Pmn2_1$ ), and when  $M = V^{5+}$  the compound is CS (space group  $P\bar{3}m1$  or  $C2/m$ ). In the NCS compounds, the polarity is caused by out of center distortions of the bridging anion in bimetallic BBUs. The bridging fluoride anion distorts to fulfill its valence, generating an NCS structures  $\Lambda$ -shaped BBU that confers polarity on the structure. The distortion that ultimately leads to the  $\Lambda$ -shaped BBU is intimately connected with the packing of the extended solid. Future examinations of synthesis methodologies of NCS could continue close study of how the local geometry of larger ETM anionic basic building units can be influenced to break inversion symmetry. Additionally, the interesting halide disorder may allow these materials to be examined for possible structural order at temperatures lower than those used in this study (100 K) and for use as solid state electrolytes of halides.

## ASSOCIATED CONTENT

### Supporting Information

Spreadsheets of bond-valence calculations, a discussion of the interpretation of the results of resonance Raman spectra, a Fourier difference map of the halide channels, a discussion of halide disorder, input and output coordinates of computational geometry optimizations, figures of selected compounds, PDF diffractograms, fitting parameters for PDF data, EDS data, powder X-ray diffraction patterns for compounds 1–8, CIF data of compounds 1–8, and the commensurate model of compound 6. This material is available free of charge via the Internet at <http://pubs.acs.org>.

## AUTHOR INFORMATION

### Corresponding Author

\*E-mail: [krp@northwestern.edu](mailto:krp@northwestern.edu).

### Author Contributions

‡M.H. and M.D.D. contributed equally and are co-first-authors. They wrote the manuscript with the assistance of the coauthors, devised experimentation and concepts, and synthesized and crystallographically characterized the compounds. E.A.P. and R.P.V.D. performed and analyzed resonance Raman spectroscopy, T.T.T. and P.S.H. performed and analyzed SHG measurements, and T.S. and A.M.R. performed and analyzed computational geometry optimizations. S.E.P.-D. assisted with powder X-ray measurements. K.R.P. was the principal investigator.

### Notes

The authors declare no competing financial interest.

## ACKNOWLEDGMENTS

This work was supported by a grant from the National Science Foundation (Solid State Chemistry Award Nos. DMR-1005827 and DMR-1307698). This work made use of the J.B. Cohen X-Ray Diffraction Facility supported by the MRSEC program of the National Science Foundation (DMR-1121262) at the Materials Research Center of Northwestern University. Single crystal X-RAY data were obtained at IMSERC at NU, which is supported with grants from NSF-NSEC, NSF-MRSEC, the Keck Foundation, the state of Illinois, and Northwestern University. Use of the Advanced Photon Source at Argonne National Laboratory was supported by the U.S. Department of Energy, Office of Science, Office of Basic Energy Sciences, under Contract No. DE-AC02-06CH11357. We would like to thank Amy Sarjeant (Northwestern University (NU)) for

significant discussions regarding the structures. We thank Karena Chapman and Kevin Beyer (Argonne National Laboratory), for assistance with PDF measurements. P.S.H. and T.T.T. thank the Welch Foundation (Grant E-1457) and the Texas Center for Superconductivity for support. E.A.P. and R.P.V.D. acknowledge the Hierarchical Materials Cluster Program at NU and the National Science Foundation Grant CHE-1152547 for support for optical measurements. T.S. is grateful to the National Science Foundation's MRSEC program (DMR-1121262) at the Materials Research Center of Northwestern University for support. A.M.R. acknowledges funding from the IGERT: Quantum Coherent Optical and Matter Systems Program (NSF Award No. 0801685). This material is based upon work supported by the National Science Foundation Graduate Research Fellowship under Grant No. DGE-1324585. Any opinions, findings, and conclusions or recommendations expressed in this material are those of the authors and do not necessarily reflect the views of the National Science Foundation.

## REFERENCES

- (1) Lippman, G. *Ann. Chim. Phys.* **1881**, *24*, 145.
- (2) Valasek, J. *Phys. Rev.* **1920**, *15*, 537.
- (3) Franken, P. A.; Hill, A. E.; Peters, C. W.; Weinreich, G. *Phys. Rev. Lett.* **1961**, *7*, 118.
- (4) Rieckhoff, K. E.; Peticolas, W. L. *Science* **1965**, *147*, 610.
- (5) Kurtz, S. K.; Perry, T. T. *J. Appl. Phys.* **1968**, *39*, 3798.
- (6) Flack, H. D. *Helv. Chim. Acta* **2003**, *86*, 905.
- (7) Chen, C. T. *Sci. Sin.* **1978**, *22*, 756.
- (8) Ye, N.; Chen, Q.; Wu, B.; Chen, C. *J. Appl. Phys.* **1998**, *84*, 555.
- (9) Pearson, R. G. *Proc. Natl. Acad. Sci. U.S.A.* **1975**, *72*, 2104.
- (10) Pauling, L. *J. Am. Chem. Soc.* **1929**, *51*, 1010.
- (11) Donakowski, M. D.; Gautier, R.; Yeon, J.; Moore, D. T.; Nino, J. C.; Halasyamani, P. S.; Poeppelmeier, K. R. *J. Am. Chem. Soc.* **2012**, *134*, 7679.
- (12) Goodey, J.; Broussard, J.; Halasyamani, P. S. *Chem. Mater.* **2002**, *14*, 3174.
- (13) Halasyamani, P. S.; Heier, K. R.; Norquist, A. J.; Stern, C. L.; Poeppelmeier, K. R. *Inorg. Chem.* **1998**, *37*, 369.
- (14) Heier, K. R.; Norquist, A. J.; Halasyamani, P. S.; Duarte, A.; Stern, C. L.; Poeppelmeier, K. R. *Inorg. Chem.* **1999**, *38*, 762.
- (15) Marvel, M. R.; Lesage, J.; Baek, J.; Halasyamani, P. S.; Stern, C. L.; Poeppelmeier, K. R. *J. Am. Chem. Soc.* **2007**, *129*, 13963.
- (16) Ra, H.-S.; Ok, K. M.; Halasyamani, P. S. *J. Am. Chem. Soc.* **2003**, *125*, 7764.
- (17) Maggard, P. A.; Stern, C. L.; Poeppelmeier, K. R. *J. Am. Chem. Soc.* **2001**, *123*, 7742.
- (18) Brock, C. P.; Dunitz, J. D. *Chem. Mater.* **1994**, *6*, 1118.
- (19) Yamamoto, H.; Katogi, S. *Appl. Phys. Lett.* **1992**, *60*, 935.
- (20) Tao, X. T.; Watanabe, T.; Shimoda, S.; Zou, D. C.; Sato, H.; Miyata, S. *Chem. Mater.* **1994**, *6*, 1961.
- (21) Tao, X. T.; Watanabe, T.; Zou, D. C.; Shimoda, S.; Usui, H.; Sato, H.; Miyata, S. *J. Polym. Sci., Part B: Polym. Phys.* **1995**, *33*, 2205.
- (22) Ostroverkhov, V.; Petschek, R. G.; Singer, K. D.; Twieg, R. J. *Chem. Phys. Lett.* **2001**, *340*, 109.
- (23) Chang, P.-H.; Chen, J.-Y.; Tsai, H.-C.; Hsiue, G.-H. *J. Polym. Sci., Part A: Polym. Chem.* **2009**, *47*, 4937.
- (24) Kaidalova, T. A.; Pakhomov, V. I.; Panin, E. S. *Koord. Khim.* **1976**, *2*, 554.
- (25) Mattes, R.; Mennemann, K.; Jaeckel, N.; Rieskamp, H.; Brockmeyer, H. J. *J. Less-Common Met.* **1980**, *76*, 199.
- (26) Hoskins, B. F.; Linden, A.; O'Donnell, T. A. *Inorg. Chem.* **1987**, *26*, 2223.
- (27) Stephens, N. F.; Lightfoot, P. *Acta Crystallogr., Sect. C* **2005**, *61*, m344.
- (28) Marvel, M. R. Doctoral, Northwestern University, 2008.
- (29) Udovenko, A. A.; Laptash, N. M. *Acta Crystallogr., Sect. B* **2012**, *68*, 602.
- (30) Nieboer, J.; Haiges, R.; Hillary, W.; Yu, X.; Richardet, T.; Mercier, H. P. A.; Gerken, M. *Inorg. Chem.* **2012**, *51*, 6350.
- (31) Harrison, W. T. A.; Nenoff, T. M.; Gier, T. E.; Stucky, G. D. *Inorg. Chem.* **1993**, *32*, 2437.
- (32) Norquist, A. J.; Heier, K. R.; Stern, C. L.; Poeppelmeier, K. R. *Inorg. Chem.* **1998**, *37*, 6495.
- (33) Kurtz, S. K.; Perry, T. T. *J. Appl. Phys.* **1968**, *39*, 3798.
- (34) 7.23A ed.; Bruker AXS Inst. Inc.: Madison, WI, 2005.
- (35) Sheldrick, G. *Acta Crystallogr., Sect. A* **2008**, *64*, 112.
- (36) Dolomanov, O. V.; Bourhis, L. J.; Gildea, R. J.; Howard, J. A. K.; Puschmann, H. *J. Appl. Crystallogr.* **2009**, *42*, 339.
- (37) Spek, A. L. *Acta Crystallogr., Sect. D* **2009**, *65*, 148.
- (38) Shao, Y.; Molnar, L. F.; Jung, Y.; Kussmann, J.; Ochsenfeld, C.; Brown, S. T.; Gilbert, A. T. B.; Slipchenko, L. V.; Levchenko, S. V.; O'Neill, D. P.; DiStasio, R. A., Jr.; Lochan, R. C.; Wang, T.; Beran, G. J. O.; Besley, N. A.; Herbert, J. M.; Yeh Lin, C.; Van Voorhis, T.; Hung Chien, S.; Sodt, A.; Steele, R. P.; Rassolov, V. A.; Maslen, P. E.; Korambath, P. P.; Adamson, R. D.; Austin, B.; Baker, J.; Byrd, E. F. C.; Dachsels, H.; Doerksen, R. J.; Dreuw, A.; Dunietz, B. D.; Dutoi, A. D.; Furlani, T. R.; Gwaltney, S. R.; Heyden, A.; Hirata, S.; Hsu, C.-P.; Kedziora, G.; Khalliulin, R. Z.; Klunzinger, P.; Lee, A. M.; Lee, M. S.; Liang, W.; Lotan, I.; Nair, N.; Peters, B.; Proynov, E. I.; Pieniazek, P. A.; Min Rhee, Y.; Ritchie, J.; Rosta, E.; David Sherrill, C.; Simmonett, A. C.; Subotnik, J. E.; Lee Woodcock, H., III; Zhang, W.; Bell, A. T.; Chakraborty, A. K.; Chipman, D. M.; Keil, F. J.; Warshel, A.; Hehre, W. J.; Schaefer, H. F., III; Kong, J.; Krylov, A. I.; Gill, P. M. W.; Head-Gordon, M. *Phys. Chem. Chem. Phys.* **2006**, *8*, 3172.
- (39) Brown, I. D. *Phys. Chem. Miner.* **1987**, *15*, 30.
- (40) Brown, I. D.; Altermatt, D. *Acta Crystallogr., Sect. B* **1985**, *41*, 244.
- (41) Brese, N. E.; O'Keeffe, M. *Acta Crystallogr., Sect. B* **1991**, *47*, 192.
- (42) Kunz, M.; Brown, I. D. *J. Solid State Chem.* **1995**, *115*, 395.
- (43) Chung, I.; Lee, B.; He, J.; Chang, R. P. H.; Kanatzidis, M. G. *Nature* **2012**, *485*, 486.
- (44) Welk, M. E.; Norquist, A. J.; Arnold, F. P.; Stern, C. L.; Poeppelmeier, K. R. *Inorg. Chem.* **2002**, *41*, 5119.
- (45) Trotter, P. J.; White, P. A. *Appl. Spectrosc.* **1978**, *32*, 323.
- (46) Bandrauk, A. D.; Truong, K. D.; Carlone, C.; Jandl, S. *Chem. Phys. Lett.* **1983**, *95*, 78.
- (47) Chen, X.; Rickard, M. A.; Hull, J. W., Jr.; Zheng, C.; Leugers, A.; Simonicic, P. *Inorg. Chem.* **2010**, *49*, 8684.
- (48) Burns, G. R.; Renner, R. M. *Spectrochim. Acta, Part a: Mol. Biomol. Spectrosc.* **1991**, *47*, 991.
- (49) Nour, E. M.; Shahada, L. *Spectrochim. Acta, Part a: Mol. Biomol. Spectrosc.* **1989**, *45*, 1033.
- (50) Sugai, S.; Saito, G. *Solid State Commun.* **1986**, *58*, 759.
- (51) Świetlik, R.; Schweitzer, D.; Keller, H. J. *Phys. Rev. B* **1987**, *36*, 6881.
- (52) Kalina, D. W.; Lyding, J. W.; Ratajack, M. T.; Kannewurf, C. R.; Marks, T. J. *J. Am. Chem. Soc.* **1980**, *102*, 7854.
- (53) Welk, M. E.; Norquist, A. J.; Stern, C. L.; Poeppelmeier, K. R. *Inorg. Chem.* **2000**, *39*, 3946.
- (54) Izumi, H. K.; Kirsch, J. E.; Stern, C. L.; Poeppelmeier, K. R. *Inorg. Chem.* **2005**, *44*, 884.
- (55) Ok, K. M.; Halasyamani, P. S.; Casanova, D.; Lluell, M.; Aleman, P.; Alvarez, S. *Chem. Mater.* **2006**, *18*, 3176.
- (56) Kirsch, J. E.; Izumi, H. K.; Stern, C. L.; Poeppelmeier, K. R. *Inorg. Chem.* **2005**, *44*, 4586.
- (57) Urusov, V. S. Z. *Kristallogr.—Cryst. Mater.* **2003**, *218*, 709.
- (58) LeBlond, N.; Mercier, H. P. A.; Dixon, D. A.; Schrobilgen, G. J. *Inorg. Chem.* **2000**, *39*, 4494.
- (59) Bertolini, J. C. *J. Emerg. Med.* **1991**, *10*, 163.
- (60) Peters, D.; Miethchen, R. *J. Fluorine Chem.* **1996**, *79*, 161.
- (61) Segel, E. B. *Chem. Health Saf.* **1996**, *7*, 18.